Astronomy & Astrophysics manuscript no. main
May 18, 2026

On the quenching of LRD X-ray emission by both Compton-thick gas and high accretion rates

Albert Sneppen[1,2], Darach Watson[1,2], James H. Matthews[3], Stuart A. Sim[4]

[1] Cosmic Dawn Center (DAWN)
[2] Niels Bohr Institute, University of Copenhagen, Jagtvej 128, DK-2200, Copenhagen N, Denmark
[3] Astrophysics, Department of Physics, University of Oxford, Keble Road, Oxford OX1 3RH, UK
[4] School of Mathematics and Physics, Astrophysics Research Centre, Queen's University Belfast, Belfast, United Kingdom

Received date / Accepted date

ABSTRACT

Little Red Dots (LRDs), candidate high-redshift supermassive black holes accreting in dense gas, remain undetected in X-rays. In previous work, we provided the first quantitative models that reproduce the optical and near-infrared spectra of LRDs with the Sirocco radiative transfer code, thereby constraining the properties of the surrounding gas. Here, we use those constraints to predict the X-ray attenuation produced by dense gas cocoons, and explore its dependence on Balmer-break strength, metallicity, intrinsic X-ray SED, and observed bandpass as a function of redshift. We find that the X-ray constraints are very tight, requiring both extinction by a Compton-thick gas column ($N_{\rm H} \sim 10^{25}\,{\rm cm}^{-2}$) with moderate metallicity (0.05–0.1 $Z_\odot$) and intrinsically weak X-ray emission (bolometric to X-ray luminosity ratio, $k_{\rm bol,X} \gtrsim 30$) as observed in high accretion rate, narrow-line AGN, to make LRDs sufficiently faint to evade detection. Intrinsically bright X-ray emitters as seen in typical broad-line AGN would be detected even behind the typical modest metallicity, Compton-thick gas columns inferred from the optical spectra. Very low metallicity objects could be detected in X-rays even with low intrinsic X-ray luminosities, suggesting that LRDs are not (currently) chemically pristine.

1. Introduction

X-rays are a powerful diagnostic of Active Galactic Nucleus (AGN) activity (Ueda et al. 2014). However, the putative AGN nature of Little Red Dots (LRDs) identified by *JWST* at high-redshift is challenged by their non-detection in deep *Chandra* X-ray data. LRDs have bolometric luminosities $L_{\rm bol} \sim 10^{43}$–$10^{45}\,{\rm erg\,s^{-1}}$ inferred from the restframe optical emission Greene et al. (2025); de Graaff et al. (2025a). For typical AGN bolometric corrections, this is in tension with their non-detection in deep X-ray measurements, with upper limits of $L_{2-10\,{\rm keV}} \lesssim (2-4)\times10^{41}\,{\rm erg\,s^{-1}}$ (Maiolino et al. 2025; Ananna et al. 2024; Yue et al. 2024; Sacchi & Bogdán 2025; Comastri et al. 2026).

LRDs are suggestive of AGN accretion because of their high surface brightness and compact sizes (Fujimoto et al. 2022; Kokorev et al. 2024; de Graaff et al. 2025b; Yanagisawa et al. 2026), and their broad emission-lines (Matthee et al. 2024; Greene et al. 2024; Juodžbalis et al. 2025). However, LRDs probe a novel radiative-transfer regime: dense gas where a Balmer break shapes the optical continuum (Inayoshi & Maiolino 2025; Naidu et al. 2025; de Graaff et al. 2025b) and electron scattering, rather than bulk kinematics, dominates the line widths (Rusakov et al. 2026; Chang et al. 2025; Nikopoulos et al. 2025). After correcting for electron-scattering, the characteristic black hole (BH) mass is $M_{\rm BH} \sim 10^6 M_\odot$, which implies accretion at close to the Eddington limit (Rusakov et al. 2026; Sneppen et al. 2026b). In particular, Sneppen et al. (2026b) showed that AGN emission mediated through optically thick, non-spherically symmetric, dense gas flows around a supermassive BH (SMBH) would unify the diverse population and simultaneously reproduce the ensemble of optical and near-infrared observables. The photoelectric absorption and scattering from such Compton-thick gas columns would be expected to depress X-ray emission (Juodžbalis et al. 2024; Maiolino et al. 2025; Rusakov et al. 2026). The extent to which the LRD X-ray weakness is driven by extreme accretion conditions (e.g. suppressed coronal emission) or by heavy obscuration, however, remains uncertain (Tortosa et al. 2026). In this work, we build on the models of Sneppen et al. (2026b,a) to quantify X-ray attenuation in the dense gas cocoons likely surrounding the early-phase SMBHs seen in LRDs and to test hard/X-ray-bright coronae versus soft/X-ray-weak coronae.

2. Model

The X-ray detectability of LRDs is set by the intrinsic coronal SED and by the transmission through the surrounding gas cocoon. We parameterize the intrinsic emission in terms of the bolometric luminosity ($L_{\rm bol}$), the X-ray bolometric correction ($k_{\rm bol,X}$), and the shape of the X-ray SED, while the attenuation is described by the X-ray transmission factor, $T_{\rm X}$. The bolometric luminosities of LRDs are increasingly constrained by large samples that map the diversity of the population (de Graaff et al. 2025a; Barro et al. 2025; Pérez-González et al. 2026) and by high-fidelity radiative transfer that reproduces their observed spectra. In this work, we compute $T_{\rm X}$ from the gas-cocoon properties inferred from such modelling.

We adopt the LRD model sequences of Sneppen et al. (2026b), computed with the Monte Carlo radiative-transfer code Sirocco (Long & Knigge 2002; Matthews et al. 2025). In these models, an increasing gas column density produces stronger Balmer breaks, here expressed as $D_{4000} = F_{\lambda=4200}/F_{\lambda=3500}$, and sets the width of electron-scattering line wings. As we quantify below, larger columns also progressively attenuate the X-ray emission. The mapping between D_{4000} and column density is non-linear, because once the gas becomes optically thick shortward of the Balmer break, the transmitted flux there declines rapidly with increasing column. Throughout this analysis, we

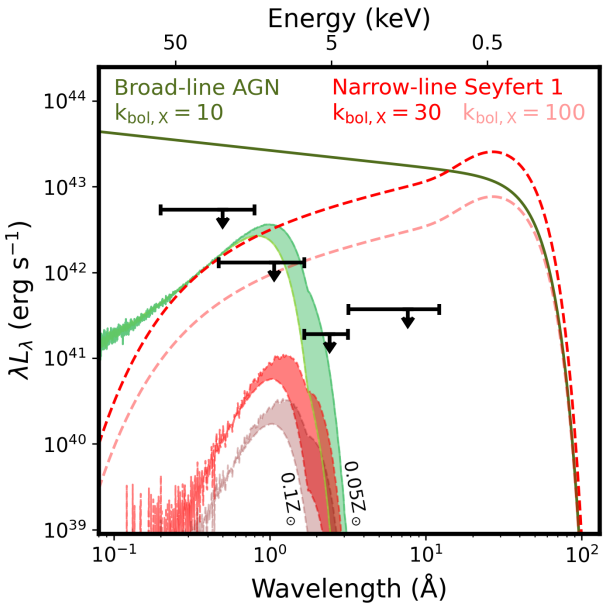

Fig. 1. The X-ray spectral energy distributions of LRDs modelled with Sirocco. X-ray upper limits for *JWST* AGNs in the *Chandra* Deep Field North and South are shown in black (Sacchi & Bogdán 2025; Comastri et al. 2026). The intrinsic X-ray templates are shown for i) a broad-line AGN similar to PDS 456 with $\Gamma = 1.8$ and $k_{bol,X} = 10$ (green) and ii) a NLS1 AGN similar to Ark 564 with a soft excess, $\Gamma = 2.4$ and $k_{bol,X} = 30$ or 100 (dashed red). The shaded region indicates the range of X-ray emission for models with Balmer-break strength $D_{4000} = 2.5$ and a metallicity $Z/Z_\odot \in [0.05; 0.1]$. A Galactic column of $N_H = 10^{21}$ cm^{-2} density is assumed for the intrinsic X-ray templates, while the Balmer-break strength $D_{4000} = 2.5$ corresponds to a column density of $N_H \sim 10^{25}$ cm^{-2}. Both intrinsic X-ray templates exceed the observational upper limits. After attenuation by the cocoon, however, the broad-line AGN X-rays are still too bright to be consistent with the data, whereas the softer NLS1 template is easily consistent with the observed upper limits.

assume that D_{4000} traces the column density, motivated by the modest dynamic range of observed D_{4000} and the presence of UV emission lines from LRDs, such as broad Lyα (Ji et al. 2026; Tang et al. 2025). If part of the UV emission instead arises outside the LRD itself, the cocoon could have a stronger Balmer break and a higher column density, allowing a higher intrinsic X-ray luminosity. For the X-ray calculations, we use the fiducial parameters, radiative-transfer model, and cocoon ionisation structure from the same model grid. The main change is that we run Sirocco in *classic mode* with weight reduction, rather than in indivisible-packet/macro-atom mode; in the current implementation, this allows a more accurate treatment of Compton heating and cooling. The X-ray photoelectric opacity is computed using the Sirocco atomic data set described by Matthews et al. (2025), which includes photoionisation cross-sections, including inner-shell cross-sections relevant for X-ray absorption (Cunto et al. 1993; Verner et al. 1993; Verner & Yakovlev 1995; Verner et al. 1996). Additional details on X-ray signatures in Monte Carlo radiative transfer and on the applicability of Sirocco to X-ray radiative transfer can be found in Sim et al. (2008) and Higginbottom et al. (2013), respectively.

Fig. 1 shows the intrinsic X-ray template spectra for a broad-line AGN (BLAGN) and a narrow-line Seyfert 1 (NLS1) on the assumption that they are little altered in such objects after leaving the innermost 10^{16} cm or so. We adopt smooth continuum shapes as intrinsic templates, with fiducial parameters motivated by AGN population properties and well-studied high-accretion-rate objects, PDS 456 and Ark 564 (Kara et al. 2017; Reeves et al. 2021). We normalize the templates using the X-ray bolometric correction $k_{bol,X} = L_{bol}/(\nu L_{2-10\,keV})$ and explore variations in $k_{bol,X}$. $k_{bol,X} \approx 10$ is consistent with bolometric corrections for low-Eddington AGN (e.g. Vasudevan & Fabian 2007), while $k_{bol,X}$ can increase to ~ 100 at near Eddington accretion rates (Lusso et al. 2012) and may be even larger if the accretion disk quenches the corona (Proga 2005). The expected hard power-law photon indices, $N(E) \propto E^{-\Gamma}$, for NLS1 and broad-line AGN are $\Gamma_{NLS1} = 2.1 \pm 0.3$ (e.g. Barua et al. 2020; Yu et al. 2023) and $\Gamma_{BLAGN} \approx 1.8$ (e.g. Ricci et al. 2018). The high-energy cut-off of this power-law is $E_{C,NLS1} \sim 30-60$ keV (Malizia et al. 2008) and $E_{C,BLAGN} = 210 \pm 36$ keV (Ricci et al. 2018). In the Compton-thick regime relevant for the LRD cocoon, harder intrinsic spectra provide more high-energy photons that can be down-scattered into the observed bandpass. They therefore predict a larger observed flux after reprocessing. The least stringent limits on the intrinsic X-ray emission are thus obtained for the softest assumed input spectrum, corresponding to the steepest power-law index and the lowest cut-off energy. Our least constraining input X-ray SED is therefore $\Gamma_{NLS1} = 2.4$ and $E_{C,NLS1} = 30$ keV.

The X-ray templates are used to bracket the intrinsic coronal SED before propagation through the cocoon. For each assumed intrinsic spectral shape and cocoon composition, the X-ray upper limits impose a lower limit on $k_{bol,X}$. We will then compare this inferred $k_{bol,X}$ with empirical AGN population relations, in which larger $k_{bol,X}$ values are typically associated with higher Eddington ratios (e.g. Duras et al. 2020; Gupta et al. 2025). Thus the inference is that normal hard, X-ray-bright coronal spectra are difficult to hide, while soft, X-ray-weak spectra characteristic of high-accretion AGN remain viable.

3. Results

For the Balmer-break strengths typical of most LRDs, $D_{4000} \in 1-10$ (de Graaff et al. 2025a; Sneppen et al. 2026b), the implied column densities are $N_H \sim 10^{24.5}-10^{25.5}$ cm^{-2}. At these column densities, the emergent X-ray spectra are characterised by a Compton hump reminiscent of Compton-thick AGN (George & Fabian 1991; Magdziarz & Zdziarski 1995; Comastri 2004) and simple X-ray models (Murphy & Yaqoob 2009; Brightman & Nandra 2011): multiple Compton scatterings redistributing higher-energy photons to lower energies and photoelectric absorption suppress the soft X-rays (see Fig. 1). Compton scattering traces the free-electron column and is dominated by the highly ionized gas interior to the Balmer-break-forming layer. Photoelectric absorption, by contrast, is dominated by bound inner-shell electrons in metals and is therefore important anywhere the gas is not fully stripped, i.e. along most of our column, including, but not limited to, the Balmer-continuum opacity region. With the magnitude of the Balmer breaks actually observed, the BLAGN template predicts X-ray fluxes that are above the observational limits, whereas the softer and less luminous NLS1 template lies below (i.e. consistent with) them.

In Fig. 2, we illustrate the parameters that shape the X-ray emission, namely the intrinsic X-ray SED, the column density, and the gas composition. Increasing the column density increases the Balmer-break strength and shifts the X-ray emission to lower energies through enhanced Compton scattering. However, the relationship between the X-ray suppression and UV attenuation as inferred from the Balmer break is complex and non-monotonic. Larger Balmer breaks do not necessarily imply

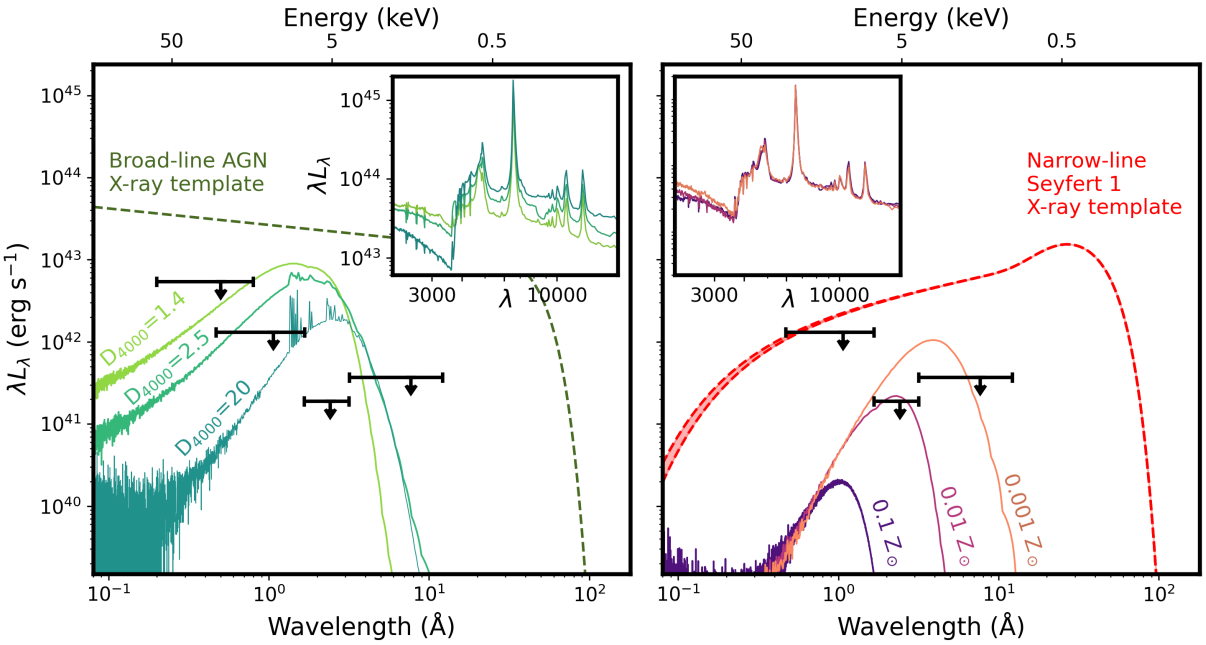

Fig. 2. X-ray Compton peaks and UV–NIR spectra (*inset*) for LRD gas cocoons with varying column density (left) and gas composition (right). In the left panel, $0.01Z_\odot$, $k_{bol,X} = 10$ and a BLAGN X-ray template is assumed; in the right panel, $D_{4000} = 2.5$, $k_{bol,X} = 50$ and a NLS1 X-ray template are assumed. Changes in composition only modestly affect the rest-frame optical spectrum via the plasma conditions, but they strongly regulate the photoelectric absorption of soft X-rays. Very low-metallicity cocoons, as expected for pristine direct-collapse black hole formation conditions, provide much lower X-ray attenuation.

weaker X-ray flux at a fixed energy below the Compton hump as Compton down-scattering redistributes photons into lower-energy bands. As a result, depending on the bandpass considered and the metallicity of the gas, the X-ray suppression, T_X, can be either greater or less than the UV attenuation suggested from the Balmer-break strength.

The cocoon composition strongly affects the degree of photoelectric absorption. An order-of-magnitude increase in metallicity leads to a factor of ~ 2 increase in the Compton peak energy and a factor of ~ 3 decrease in the peak transmitted fraction. These emergent spectral properties depend non-linearly on metallicity, because the transmitted spectrum is shaped by exponential photoelectric attenuation and Compton reprocessing. The underlying X-ray photoelectric optical depth, τ_X, however, scales approximately linearly with metallicity, since absorption at the relevant X-ray energies is dominated by metals. Equivalently, the solar-abundance-equivalent X-ray column density is $N_{H_X(Z)} = (\tau_X/\tau_{X_\odot})N_H \sim (Z/Z_\odot)N_H$. Very low metallicities, either pristine formation values $Z/Z_\odot \lesssim 10^{-5}$ invoked in direct-collapse black-hole scenarios (e.g. Clark et al. 2008; Cenci & Habouzit 2025), or enriched values $Z/Z_\odot \lesssim 5\times10^{-3}$ (Pacucci et al. 2026), imply weak photoelectric absorption and therefore only modest attenuation in the observed-frame 0.5–5 keV band. The lack of detection in X-rays therefore suggests that the gas in LRDs is not extremely metal poor, if LRDs have NLS1 or brighter AGN at their hearts.

No spectroscopically-confirmed LRD, defined by the presence of a Balmer break and broad lines, has yet been significantly detected in X-rays, although a few phenomenologically similar compact red sources have been detected in X-rays (Fu et al. 2025; Hviding et al. 2026; Kocevski et al. 2024). Deep-field limits from *Chandra* are stringent, with a combined limit of $L_{1-10\,\mathrm{keV}} \lesssim (2{-}4)\times10^{41}$ erg s^{-1} (Maiolino et al. 2025; Comastri et al. 2026) on classical LRDs. The Rosetta stone LRD alone has a restframe X-ray limit of $L_{2-10\,\mathrm{keV}} < 2.9\times10^{41}$ erg s^{-1} to be compared with a bolometric luminosity three orders of magnitude larger at $\sim 3\times10^{44}$ erg s^{-1}. This is despite a modest Balmer break, $D_{4000} \sim 2$. This combination is examined in Fig. 1, where a gas cocoon with a column density of $N_H = 10^{25}$ cm^{-2} produces a Balmer break with a similar strength to the Rosetta Stone object in the Sirocco models. A broad-line AGN X-ray template with $k_{\mathrm{bol,X}} = 10$, in this model transmits enough X-rays to contravene the observational upper limits. By contrast, a narrow-line Seyfert 1 X-ray template is consistent with the upper limits for standard bolometric corrections $k_{\mathrm{bol,X}} \sim 10{-}100$. This conclusion is conditional on the assumed intrinsic X-ray SED and cocoon properties, but within our fiducial models the key dependence is the metallicity of the absorbing gas. The limited LRD host metallicities from narrow-line ratios suggest metallicities in the range, $\sim 0.02 - 0.2\,Z_\odot$ (Juodžbalis et al. (2024); Ivey et al. (2026), Nikopoulos et al., in preparation). For an NLS1-like X-ray template and metallicities representative of the lower-metallicity part of the population, $\sim 0.04Z_\odot$, the limits imply $k_{\mathrm{bol,X}} \gtrsim 30$. Such high bolometric corrections are within the scatter of standard AGN relations, but on a population-level would suggest Eddington-ratios near unity; $\gtrsim 0.1\,L_{\mathrm{edd}}$ (Vasudevan & Fabian 2007), $\gtrsim 0.3\,L_{\mathrm{edd}}$ (Gupta et al. 2025) and/or $\gtrsim 0.6\,L_{\mathrm{edd}}$ (Duras et al. 2020). Further, a metallicity as low as $\lesssim 0.01\,Z_\odot$ would shift the Compton peak into the tightly constrained soft X-ray band (Fig. 2), requiring $k_{\mathrm{bol,X}} \gtrsim 100$ as rarely seen (Martocchia et al. 2017).

4. Predictions and conclusions

We have tested whether intrinsic AGN X-ray templates are compatible with the current X-ray upper limits for LRDs. The gas columns required to reproduce their optical and near-infrared SEDs naturally produce substantial X-ray attenuation, but in our fiducial models this attenuation is generally insufficient to hide a normal hard, X-ray-bright corona. Metallicity remains a major

uncertainty in the degree of soft X-ray flux suppression, while the hard X-ray emission at rest-frame energies $\gtrsim 10$ keV is governed mainly by the column density and the intrinsic X-ray SED. Non-detections in the *Chandra* deep fields even in circumstances with favourable redshift/bandpass, low metallicities and modest columns, suggest that i) the intrinsic X-ray SEDs of LRDs are soft and/or ii) LRDs are intrinsically weak X-ray sources relative to their bolometric luminosities (e.g. Duras et al. 2020), consistent with high accretion rate AGN. Relative to the higher energy Compton hump of standard AGN peaking at $\sim 10-30$ keV (Zhu et al. 2021), the LRD model X-rays can peak at lower energies of 4–7 keV due to the combination of high densities, which enhance Compton scattering, and lower metallicities, which reduce photoelectric absorption. The Sirocco modelling framework makes several predictions for X-ray detectability.

1. Mild Balmer-break LRD systems, particularly at low metallicities with $\lesssim 0.001-0.05 Z_{\odot}$, exhibit only mild soft X-ray suppression and are therefore promising targets for X-ray searches. Systems with small D_{4000} and low metallicities (e.g. Jades-GN 1181-73488, Nikopoulos et al. in preparation) are particularly attractive candidates. We note, that this object has a marginal X-ray detection (Maiolino et al. 2025).
2. Objects with extremely low metallicities and moderate column densities, such as those invoked for a Direct Collapse Black Hole interpretation of LRDs with $Z \ll 10^{-2} Z_{\odot}$ and a few $10^{25} \mathrm{cm}^{-2}$ (Pacucci et al. 2026), are not strongly suppressed in the *Chandra* bands. For typical $k_{\mathrm{bol,X}}$, the X-ray non-detections therefore disfavour pristine absorbing gas.
3. A population of LRDs with very strong Balmer breaks and narrow electron-scattering wings should be extremely X-ray weak: the large columns required to reprocess the broad wings, $N_{\mathrm{H}} \gtrsim 5 \times 10^{25}\,\mathrm{cm}^{-2}$, can suppress X-rays even at low metallicity.
4. Although LRDs can be labelled as 'type 1' AGN due to their broad lines, the broad wings may instead be produced by electron scattering rather than by an unobscured broad-line region. In that case, the broad lines are evidence for large scattering columns, consistent with strong obscuration in both the UV and X-rays, rather than evidence against it.
5. Standard AGN luminosity relations $L_{2\,\mathrm{keV}}-L_{2500\,\text{Å}}$ (Lusso et al. 2010) are thrown off in LRDs because dense gas can attenuate *both* the UV and X-ray emission, which easily introduces more than an order-of-magnitude systematic shift and scatter in relations between these luminosities. For the same reason, bolometric corrections calibrated on unobscured local AGN are unlikely to be reliable. Comparisons to empirically inferred or radiative-transfer-based bolometric luminosities, or to the optical luminosity where much of the reprocessed emission appears to emerge (Greene et al. 2025), are likely to be more informative.

We emphasize that X-ray non-detections alone cannot rule out a corona-free accretion state (which would be the ultimate $k_{\mathrm{bol,X}}$). Our constraints therefore apply primarily to AGN-like coronal templates: for such input spectra, the cocoon columns inferred from the optical spectra predict some X-ray weakness due to attenuation but that is generally insufficient to hide normal broad-line AGN X-ray output.

Acknowledgements. The authors would like to thank Giorgos Nikopoulos for helpful discussions. AS, DW, & SAS are funded in part by the European Union (ERC, HEAVYMETAL, 101071865). Views and opinions expressed are, however, those of the authors only and do not necessarily reflect those of the European Union or the European Research Council. Neither the European Union nor the granting authority can be held responsible for them. JHM acknowledges funding from a Royal Society University Research Fellowship (URFR1221062). SAS is supported by the UK's Science and Technology Facilities Council (STFC, respectively grant ST/V001000/1 and ST/X00094X/1).

References

Ananna, T. T., Bogdán, Á., Kovács, O. E., Natarajan, P., & Hickox, R. C. 2024, ApJ, 969, L18
Barro, G., Perez-Gonzalez, P. G., Kocevski, D., et al. 2025, arXiv e-prints, arXiv:2512.15853
Barua, S., Jithesh, V., Misra, R., et al. 2020, MNRAS, 492, 3041
Brightman, M. & Nandra, K. 2011, MNRAS, 413, 1206
Cenci, E. & Habouzit, M. 2025, MNRAS, 542, 2597
Chang, S.-J., Gronke, M., Matthee, J., & Mason, C. 2025, arXiv e-prints, arXiv:2508.08768
Clark, P. C., Glover, S. C. O., & Klessen, R. S. 2008, ApJ, 672, 757
Comastri, A. 2004, in Astrophysics and Space Science Library, Vol. 308, Supermassive Black Holes in the Distant Universe, ed. A. J. Barger, 245
Comastri, A., Lanzuisi, G., Vito, F., et al. 2026, A&A, 706, A302
Cunto, W., Mendoza, C., Ochsenbein, F., & Zeippen, C. J. 1993, A&A, 275, L5
de Graaff, A., Hviding, R. E., Naidu, R. P., et al. 2025a, arXiv e-prints, arXiv:2511.21820
de Graaff, A., Rix, H.-W., Naidu, R. P., et al. 2025b, arXiv e-prints, arXiv:2503.16600
Duras, F., Bongiorno, A., Ricci, F., et al. 2020, A&A, 636, A73
Fu, S., Zhang, Z., Jiang, D., et al. 2025, arXiv e-prints, arXiv:2512.02096
Fujimoto, S., Brammer, G. B., Watson, D., et al. 2022, Nature, 604, 261
George, I. M. & Fabian, A. C. 1991, MNRAS, 249, 352
Greene, J. E., Labbe, I., Goulding, A. D., et al. 2024, ApJ, 964, 39
Greene, J. E., Setton, D. J., Furtak, L. J., et al. 2025, arXiv e-prints, arXiv:2509.05434
Gupta, K. K., Ricci, C., Tortosa, A., et al. 2025, ApJ, 990, 86
Higginbottom, N., Knigge, C., Long, K. S., Sim, S. A., & Matthews, J. H. 2013, MNRAS, 436, 1390
Hviding, R. E., de Graaff, A., Liu, H., et al. 2026, arXiv e-prints, arXiv:2601.09778
Inayoshi, K. & Maiolino, R. 2025, ApJ, 980, L27
Ivey, L. R., D'Eugenio, F., Maiolino, R., et al. 2026, arXiv e-prints, arXiv:2604.09177
Ji, X., Pezzulli, G., D'Eugenio, F., et al. 2026, arXiv e-prints, arXiv:2604.03370
Juodžbalis, I., Ji, X., Maiolino, R., et al. 2024, MNRAS, 535, 853
Juodžbalis, I., Maiolino, R., Baker, W. M., et al. 2025, arXiv e-prints, arXiv:2504.03551
Kara, E., García, J. A., Lohfink, A., et al. 2017, MNRAS, 468, 3489
Kocevski, D. D., Finkelstein, S. L., Barro, G., et al. 2024, arXiv e-prints, arXiv:2404.03576
Kokorev, V., Caputi, K. I., Greene, J. E., et al. 2024, ApJ, 968, 38
Long, K. S. & Knigge, C. 2002, ApJ, 579, 725
Lusso, E., Comastri, A., Simmons, B. D., et al. 2012, MNRAS, 425, 623
Lusso, E., Comastri, A., Vignali, C., et al. 2010, A&A, 512, A34
Magdziarz, P. & Zdziarski, A. A. 1995, MNRAS, 273, 837
Maiolino, R., Risaliti, G., Signorini, M., et al. 2025, MNRAS[arXiv:2405.00504]
Malizia, A., Bassani, L., Bird, A. J., et al. 2008, MNRAS, 389, 1360
Martocchia, S., Piconcelli, E., Zappacosta, L., et al. 2017, A&A, 608, A51
Matthee, J., Naidu, R. P., Brammer, G., et al. 2024, ApJ, 963, 129
Matthews, J. H., Long, K. S., Knigge, C., et al. 2025, MNRAS, 536, 879
Murphy, K. D. & Yaqoob, T. 2009, MNRAS, 397, 1549
Naidu, R. P., Matthee, J., Katz, H., et al. 2025, arXiv e-prints, arXiv:2503.16596
Nikopoulos, G. P., Watson, D., Sneppen, A., et al. 2025, arXiv e-prints, arXiv:2510.06362
Pacucci, F., Ferrara, A., & Kocevski, D. D. 2026, arXiv e-prints, arXiv:2601.14368
Pérez-González, P. G., Barro, G., Carniani, S., et al. 2026, arXiv e-prints, arXiv:2602.20247
Proga, D. 2005, ApJ, 630, L9
Reeves, J. N., Braito, V., Porquet, D., et al. 2021, MNRAS, 500, 1974
Ricci, C., Ho, L. C., Fabian, A. C., et al. 2018, MNRAS, 480, 1819
Rusakov, V., Watson, D., Nikopoulos, G. P., et al. 2026, Nature, 649, 574
Sacchi, A. & Bogdán, Á. 2025, ApJ, 989, L30
Sim, S. A., Long, K. S., Miller, L., & Turner, T. J. 2008, MNRAS, 388, 611
Sneppen, A., Matthews, J. H., Watson, D., et al. 2026a, arXiv e-prints, arXiv:2604.09399
Sneppen, A., Watson, D., Matthews, J. H., et al. 2026b, arXiv e-prints, arXiv:2601.18864
Tang, M., Stark, D. P., Plat, A., et al. 2025, arXiv e-prints, arXiv:2505.06359
Tortosa, A., Ricci, C., Du, P., et al. 2026, arXiv e-prints, arXiv:2603.10162
Ueda, Y., Akiyama, M., Hasinger, G., Miyaji, T., & Watson, M. G. 2014, ApJ, 786, 104
Vasudevan, R. V. & Fabian, A. C. 2007, MNRAS, 381, 1235
Verner, D. A., Ferland, G. J., Korista, K. T., & Yakovlev, D. G. 1996, ApJ, 465, 487
Verner, D. A. & Yakovlev, D. G. 1995, A&AS, 109, 125
Verner, D. A., Yakovlev, D. G., Band, I. M., & Trzhaskovskaya, M. B. 1993, Atomic Data and Nuclear Data Tables, 55, 233
Yanagisawa, H., Ouchi, M., Golubchik, M., et al. 2026, arXiv e-prints, arXiv:2601.06015
Yu, Z., Jiang, J., Bambi, C., et al. 2023, MNRAS, 522, 5456
Yue, M., Eilers, A.-C., Ananna, T. T., et al. 2024, ApJ, 974, L26
Zhu, S. F., Timlin, J. D., & Brandt, W. N. 2021, MNRAS, 505, 1954

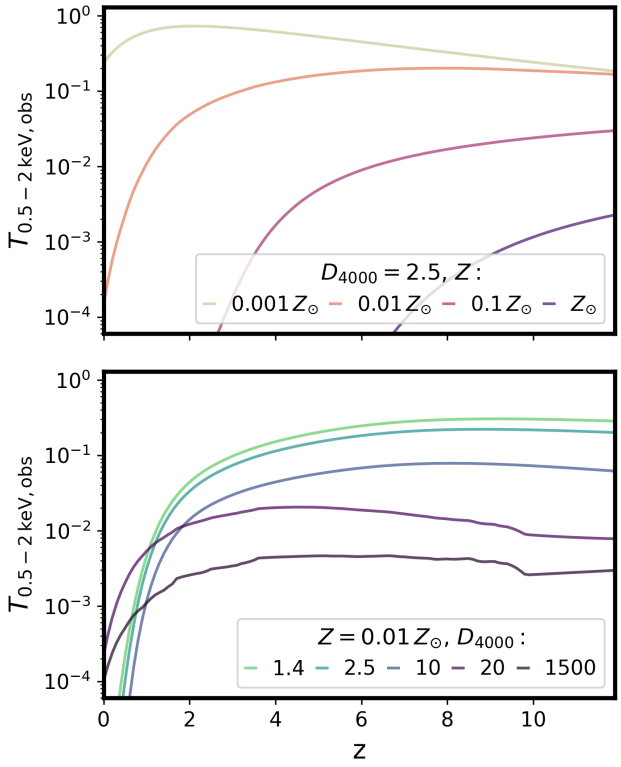

Fig. A.1. X-ray transmitted fraction, $T_{0.5-5\,\mathrm{keV,obs}}$, as a function of redshift, metallicity and cocoon column density, parameterized by the Balmer-break strength D_{4000}. The highest transmission occurs for low metallicity, modest redshift, and weak Balmer breaks, whereas metal-enriched cocoons at low redshift strongly suppress X-rays by photo-electric absorption. In the most optically thick regimes, high ionisation X-ray emission lines begin to dominate the transfer function, which produces 'wiggles' as the bandpass moves over ionised lines.

Appendix: Band-integrated transmission fraction

In Fig. A.1, we quantify the band-integrated transmission fraction as a function of the redshift, z, for different metallicities and cocoon column densities. The conditions for minimal X-ray suppression occur at intermediate redshifts, $z \sim 2$–3, low metallicities, $Z \lesssim 0.1$, and low column densities ($D_{4000} \sim 1$, e.g., SEDs with continuum inflection near the Balmer break wavelength). In fact, Compton down-scattering can even redistribute photons into the soft bands and increase the soft-band luminosity relative to the intrinsic emission. Lower-redshift objects can be strongly obscured by photoelectric absorption because we are observing their softer X-rays. Fortunately, objects within the *Chandra* Deep Fields, such as Jades-GN 1181-73488 (Juodžbalis et al. 2025) and the Rosetta Stone LRD (Juodžbalis et al. 2024), broadly fulfil such criteria and are relatively bright, providing useful case studies for comparison with deep observational limits.